Inorganic Chemistry

Article

pubs.acs.org/IC

From T2,2@Bmmim to Alkali@T2,2@Bmmim Ivory Ball-like Clusters: Ionothermal Syntheses, Precise Doping, and Photocatalytic Properties

Cheng-Feng Du,[†,‡] Jian-Rong Li,[*,†] Bo Zhang,[†,‡] Nan-Nan Shen,[†,‡] and Xiao-Ying Huang[†]

[†]State Key Laboratory of Structural Chemistry, Fujian Institute of Research on the Structure of Matter, Chinese Academy of Sciences, Fuzhou, Fujian, 350002, People's Republic of China

[‡]University of Chinese Academy of Sciences, Beijing, 100049, People's Republic of China

Supporting Information

ABSTRACT: Presented here are the syntheses, structures, and properties of an In-Sn-Se compound based on a ternary super-supertetrahedral T2,2 cluster nested by Bmmim cations and two of its alkali-doped quaternary analogues. By means of a one-pot ionothermal method, an alkali metal ion (Cs^+ or Rb^+) could be precisely doped into the central cavity of the cluster, forming an alkali@T2,2@Bmmim quaternary cluster. Remarkably, the undoped compound exhibited excellent stability and visible light photodegradation ability over a wide range of pH, especially in acidic conditions.

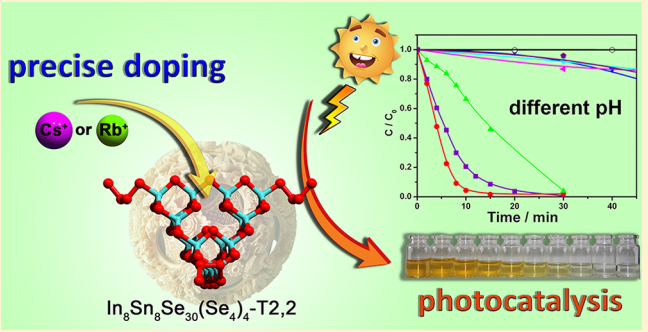

INTRODUCTION

Chalcogenidometallate compounds, normally being semiconductors, have caught much attention due to their potential applications in energy harvest, catalysis, light emitting, sensing, and so on.[1] Doping is one of the most effective ways to achieve the various applications of semiconductors.[1a,d,2] By artificially introducing "impurities", the molecular and electronic structures of semiconducting materials can be altered and some intriguing physical and chemical properties can be realized.[3] For many practical applications, precise and uniform doping is very much needed yet is a challenging task.[1a,3a]

Recently, Wu et al. found that the precise doping could be achieved in a class of crystalline compounds based on nanosized coreless clusters.[4] These clusters belong to a class of so-called chalcogenido supertetrahedral clusters with a well-defined chemical composition. Since the cluster is in a single-crystalline nature, they were able to probe the doping positions precisely via single-crystal X-ray diffraction analysis. Through a two-step synthetic strategy, the Cu^+ and Mn^{2+} were exactly doped at the vacant site of the coreless T5 $[Cd_6In_{28}S_{52}(SH)_4]$ supertetrahedral cluster, and the dopants brought tunable photoelectric response behavior and photoluminescence properties relative to the pristine host materials.[4,5] Compared to colloidal nanoparticles, in which the doped atoms tend to randomly distribute in the matrix,[6] such precise doping of heterogeneous atoms in nanosized clusters is unique, but still limited to thiometallate clusters, and the dopant is restricted to transition metal ions. Compared to sulfides, the heavy chalcogenides such as selenides are desirable for their photoconductivity and electronic band gap tunability,[1b,7] which make them be used extensively in xerography, semiconductor devices, and photovoltaic cells.[8] For this reason, an accessible way of preparing selenide nanoclusters and carefully evaluating their structure−property relationship is desperately needed for materials design.

Room-temperature ionic liquids (RTILs) have been widely used in material synthesis.[9] Our group has developed a new synthetic route toward chalcogenido compounds with a discrete nanosized cluster in RTILs.[10] In this report, a core−shell T2,2 cluster-based layered structure with polyselenium Se_4 chains as linker was first obtained by means of a one-pot ionothermal method, namely, $(Bmmim)_8In_8Sn_8Se_{30}(Se_4)_2$ (**1**, denoted as T2,2@Bmmim, Bmmim = 1-butyl-2,3-dimethyl imidazolium). Further, the alkali metal ions could be precisely doped into the central cavity of the nanosized clusters and form an ivory ball-like core−shell−shell structure, namely, quaternary A@T2,2@Bmmim, (A = Cs (**2**) and Rb (**3**)). To the best of our knowledge, this is the first report of ternary In-Sn-Se and quaternary A-In-Sn-Se T2,2 clusters. The visible light photodegradation of organic dye studies showed that **1** can retain stability over a wide pH range from 1.5 to 10, and an acceleration of degradation rate of MO for **1** in acidic conditions was observed.

EXPERIMENTAL SECTION

Materials and Physical Measurements. In (99.5%) powder and hydrazine hydrate (85%) were purchased from Sinopharm Chemical

Received: March 23, 2015
Published: June 2, 2015

DOI: 10.1021/acs.inorgchem.5b00652
Inorg. Chem. 2015, 54, 5874−5878

Table 1. Crystal Data and Structure Refinement Parameters for Compounds 1−3

	1	2	3
formula	$C_{72}H_{136}In_8N_{16}Se_{38}Sn_8$	$C_{72}H_{136}CsIn_9N_{16}Se_{38}Sn_7$	$C_{72}H_{136}In_9N_{16}RbSe_{38}Sn_7$
M_r (g mol^{-1})	6094.53	6223.57	6176.13
temp (K)	100(2)	100(2)	100(2)
λ (Å)	1.5418	1.5418	1.5418
crystal system	tetragonal	tetragonal	tetragonal
space group	$I4_1/a$	$I4_1/a$	$I4_1/a$
D_{calcd} (g cm^{-3})	2.787	2.843	2.827
a (Å)	19.59310(10)	19.6437(2)	19.6218(4)
c (Å)	37.8365(8)	37.7046(8)	37.6897(9)
V (Å^3)	14525.0(3)	14549.3(4)	14511.2(5)
Z	4	4	4
μ (mm^{-1})	31.866	33.638	32.205
R_{int}	0.0324	0.0250	0.0318
$R_1{}^a$ [$I > 2\sigma(I)$]	0.0472	0.0418	0.0423
$wR_2{}^b$ [$I > 2\sigma(I)$]	0.1235	0.1246	0.1221
goodness of fit	1.016	1.003	1.007

$^aR_1 = \sum(F_o - F_c)/\sum F_o$. $^bwR_2 = [\sum w(F_o^2 - F_c^2)^2/\sum w(F_o^2)^2]^{1/2}$.

Reagent, $Na_2SnO_3{\cdot}4H_2O$ (AR) and selenium (AR) powder were purchased from Tianjin Yingda Rare Chemical Reagent, (Bmmim)Cl (99%) was purchased from Lanzhou Greenchem ILS, LICP. CAS. China, and CsCl (AR) and RbCl (AR) were purchased from Aladdin, respectively. All the chemicals were used without further purification. Powder X-ray diffraction (PXRD) patterns were recorded on a Rigaku Miniflex-II diffractometer by using Cu Kα radiation. Elemental analysis was performed on a German Elementary Vario EL III instrument. Elemental ratios of In and Sn were determined by inductively coupled plasma (ICP)-atomic emission spectrometry (AES) by using an Ultima 2 instrument. Thermogravimetric analysis (TGA) was carried out on a NETZSCH STA 449F3 unit at a heating rate of 10 K min^{-1} under a N_2 atmosphere. Optical diffuse reflectance spectra were recorded at room temperature on a Shimadzu UV-2600 UV−vis spectrophotometer, with a $BaSO_4$ plate as a standard (100% reflectance). The absorption data were calculated from reflectance spectra by using the Kubelka−Munk function $F(R_\infty)$: $F(R_\infty) = (1 - R_\infty)^2/2R_\infty$, where R_∞ is the reflection coefficient of the sample.[11]

Syntheses of $(Bmmim)_8In_8Sn_8Se_{30}(Se_4)_2$ (1). The synthesis of **1** was carried out by a one-pot ionothermal method. In a typical reaction, 0.115 g (1 mmol) of In, 0.267 g (1 mmol) of $Na_2SnO_3{\cdot}3H_2O$, and 0.474 g (6 mmol) of Se powder were mixed with 1 g (5.3 mmol) of (Bmmim)Cl and 1 mL of hydrazine hydrate (85%). The mixture was transferred to a 20 mL Teflon-lined steel autoclave and kept at 150 °C for 6 days. After being cooled to room temperature, the product was washed with ethanol. Then, the orange-red block crystals of **1** were obtained (Yield: 0.401 g, ∼53% based on Sn. Elemental analysis, calcd. (%) for $C_{72}H_{136}In_8N_{16}Se_{38}Sn_8$: C 14.19, H 2.25, N 3.68; found: C 14.25, H 2.38, N 3.95).

Syntheses of Alkali Metal-Doped $(Bmmim)_8AIn_9Sn_7Se_{30}(Se_4)_2$ (A = Cs for 2 and Rb for 3). To prepare the alkali metal ion doped compounds A@T2,2@Bmmim, similar conditions were applied, except that the alkali chloride (ACl, A = Cs^+ and Rb^+) was added into the reactions for **2** and **3**, respectively. Typically, 0.115 g (1 mmol) of In, 0.267 g (1 mmol) of $Na_2SnO_3{\cdot}3H_2O$, 0.474 g (6 mmol) of Se powder, and 0.5 mmol of ACl were mixed with 1 g (5.3 mmol) of (Bmmim)Cl and 1 mL of hydrazine hydrate (85%). The mixture was transferred to a 20 mL Teflon-lined steel autoclave and kept at 150 °C for 6 days. After being cooled to room temperature, the product was washed with ethanol. The block crystals of **2** (Yield: 0.393 g, ∼60% based on Sn. Elemental analysis, calcd. (%) for $C_{72}H_{136}CsIn_9N_{16}Se_{38}Sn_7$: C 13.90, H 2.20, N 3.60; found: C 13.72, H 2.19, N 3.53) and **3** (Yield: 0.498 g, ∼76% based on Sn. Elemental analysis, calcd. (%) for $C_{72}H_{136}RbIn_9N_{16}Se_{38}Sn_7$: C 14.00, H 2.22, N 3.63; found: C 14.22, H 2.32, N 3.66) were obtained.

X-ray Crystal Structure Determination. The intensity data were collected on a SuperNova CCD diffractometer for **1**, **2**, and **3** at 100 K with graphite-monochromated Cu Kα radiation (λ = 1.5418 Å). The structures were solved by direct methods and refined by full-matrix least-squares on F^2 using the SHELX2013 program package.[12] Some restraints (DFIX, SIMU, and SADI) were applied to the disordered $[Bmmim]^+$ to obtain the chemical-reasonable models and reasonable atomic displacement parameters. The occupancy ratio of In/Sn for each metal ion site in compound **1** was set to be 0.50/0.50 according to the results of EDX and ICP analyses, whereas, in compounds **2** and **3**, the occupancy ratio of In/Sn for each metal ion site was set to be 0.5625/0.4375. The crystal data and details of refinements of compounds **1**−**3** are depicted in Table 1.

Detailed Process of Dye Photodegradation. The photodegradation reactions under visible light irradiation (420−780 nm) for the degradation of the MO were performed in a glass reactor with a flat section of 18 cm^2. A 50 W Xe lamp (Perfect Light, PLS-SXE300UV) with a 420 nm cutoff filter was used as illuminating source, ensuring irradiation with visible light only. The distance between the Xe lamp and the reactor is 20 cm. The pH of MO solutions is adjusted with diluted HCl and NaOH aqueous solutions. Powdered photocatalysts (25 mg) were suspended in 100 mL of MO (10^{-5} mol L^{-1}) aqueous solution and stirred for 60 min in the dark before irradiation to reach the adsorption/desorption equilibrium. About 5 mL of the suspension was continually taken from the reaction cell at certain time intervals during the irradiation and centrifuged (Anke, TGL-16C). The resulting solution was analyzed on a Shimadzu UV-2600 UV−vis spectrophotometer. The percentage of degradation is reported as C/C_0, where C is the main peak of the absorption of methyl orange at each irradiated time interval at wavelength 464 nm and C_0 is the absorption of the starting concentration when the adsorption/desorption equilibrium was achieved.

RESULTS AND DISCUSSION

Description of Crystal Structures of 1−3. All the compounds belong to the $I4_1/a$ space group. Taking compound **1** as an example, the structure features an infinite 2D-anionic $[In_8Sn_8Se_{30}(Se_4)_2]_n^{2n-}$ layer composed of $In_8Sn_8Se_{34}$-T2,2 super-supertetrahedral clusters interconnected by polyselenium Se_4 chains along the ab plane (Figure S1a, Supporting Information).[13] The asymmetric unit is composed of four $[MSe_4]$ tetrahedra (M = 0.5In + 0.5Sn), two $[Bmmim]^+$ cations, and half of the polyselenium Se_4 chain. Since the In^{3+} and Sn^{4+} atoms are isoelectronic, they cannot be distinguished directly by X-ray diffraction. The In/Sn ratios in the clusters were initially established to be 1:1 by energy-dispersive X-ray spectroscopy (EDX) and confirmed by ICP-AES. In a

DOI: 10.1021/acs.inorgchem.5b00652
Inorg. Chem. 2015, 54, 5874−5878

$In_8Sn_8Se_{34}$-T2,2 cluster, the [MSe_4] tetrahedra are interconnected to each other by sharing vertical Se atoms to form a hollow cage structure (Figure 1a). On the basis of the results of

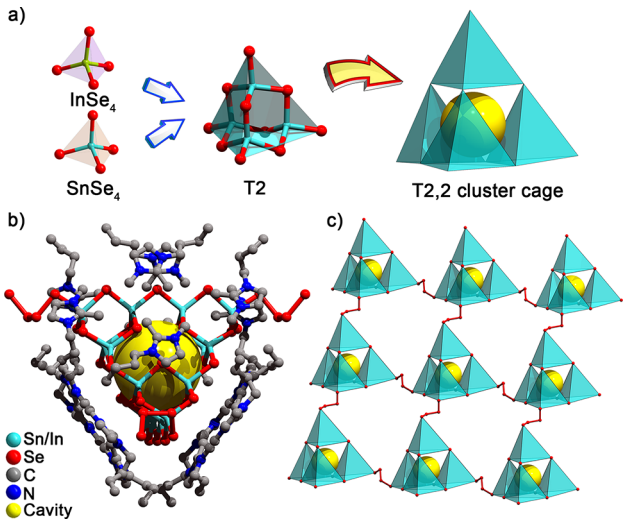

Figure 1. (a) The $In_8Sn_8Se_{34}$-T2,2 cluster built up of $InSe_4$ and $SnSe_4$ tetrahedra. (b) The T2,2 cluster with [Bmmim]$^+$ cations shell. (c) An anionic layer of **1** constructed by interconnecting the $In_8Sn_8Se_{34}$-T2,2 clusters via Se_4 chains.

structural refinements and the electroneutrality principle, the atomic site at the center of the supertetrahedron is vacant, which was also confirmed by EDX and elemental analysis.[6c] To date, the only cases of a T2,2 cluster were $In_{16}S_{32}$ in ICF-22 InS-Li and $Ga_{13.32}Ge_{2.68}S_{32}$, $Ga_{8.52}Sn_{7.48}S_{32}$, $In_{10.76}Ge_{5.24}S_{32}$, $Ga_{6.92}Sn_{9.08}Se_{32}$ in UCR-22 series.[14] Hereby, the ternary T2,2 cluster simultaneously containing In and Sn was obtained for the first time. Noteworthy, it is also the first case that the polyselenium Se_4 chain was combined with the supertetrahedral cluster. The layers are further packed into a supramolecular three-dimensional structure along the *c* axis, in which the [Bmmim]$^+$ cations filled in the interlaminar spaces as the charge compensator (Figure S1b, Supporting Information), accompanied by the hydrogen-bonding interactions and electrostatic interactions between the clusters and [Bmmim]$^+$ cations. Interestingly, the [Bmmim]$^+$ cations completely enclose every coreless $In_8Sn_8Se_{34}$-T2,2 cluster and form a double-shell ivory ball-like T2,2@Bmmim cage (Figure 1b).

In an ideal T4 cluster, there is a chalcogen core, and all the other chalcogen atoms are located on faces and edges. The four face-centers are occupied by metal atoms, which are nearest to the central atom, thus affording an electropositivity environment for charge compensation (Figure 2a). However, in the $In_8Sn_8Se_{34}$-T2,2 cluster, the central atom and its four nearest neighbor metals are missing. Due to Pauling rule, such a coreless feature ensures that all cations have tetrahedral coordination and all anions have bicoordination.[14a] The 12 selenium atoms located on faces then become the closest sites to the center (Figure 2b). Since the $In_8Sn_8Se_{34}$-T2,2 cluster cage is nearly 1.6 nm in size and possesses a negative central cavity, we suspected that the void core site in the $In_8Sn_8Se_{34}$-T2,2 cluster could be filled with a third metal ion (Cs^+ and Rb^+ here) with the appropriate valence state and ionic radius. Indeed, two new quaternary compounds could be prepared through a relatively mild one-pot ionothermal reaction. For **2** and **3**, the In/Sn ratios in the formulas are altered from 8:8 to

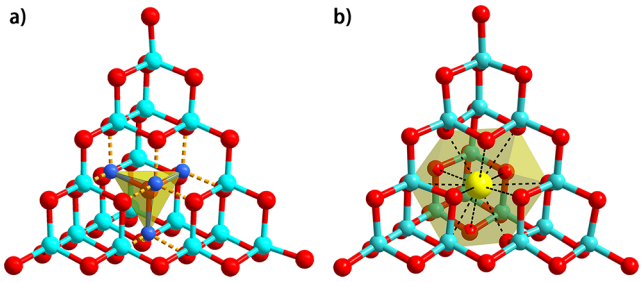

Figure 2. (a) An ideal T4 cluster. Yellow polyhedron denotes the polyhedral core of the chalcogen center and the nearest four metal atoms (blue balls). (b) The $In_8Sn_8Se_{34}$-T2,2 cluster with a central cavity. Yellow ball denotes the central site, and black dashed line shows its 12 nearest selenium atoms.

9:7 to maintain the electroneutrality of the resulting compounds, which were confirmed by ICP (for details, see the Supporting Information). We also tried to dope other ions with higher valence state such as alkaline earth ions (Ca^{2+}, Sr^{2+}) and transition metal ions (Mn^{2+}, Cu^{2+}) into the compound **1**, but failed.

Powder X-ray Diffraction Analyses, Thermal Properties, and Optical Properties. The phase purity of the products was confirmed by PXRD patterns (Figure 3). Thermal

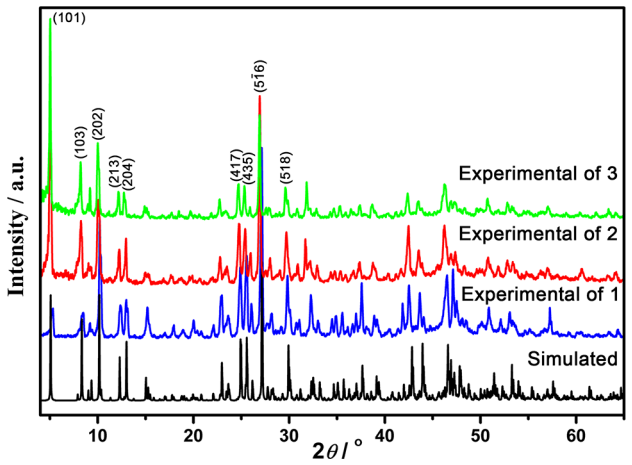

Figure 3. PXRD patterns of compounds **1**−**3** (top) are comparable with the simulated from the single-crystal X-ray data of **1** (bottom).

stabilities of **1**, **2**, and **3** were investigated on pure samples at a heating rate of 10 K min^{-1} in a N_2 atmosphere from 30 to 450 °C for **1** and 30 to 500 °C for **2** and **3**. As shown in Figure S5 (Supporting Information), the TGA curves of these compounds displayed multiple steps of weight losses from 250 to 400 °C, which are in correspondence with the losses of organic components and H_2Se molecules. The post-TGA residues were identified as the mixture of In_2Se_3 and $SnSe_2$ phases (Figure S4, Supporting Information) by PXRD.

To further investigate the doping effect of alkali metal ions, optical diffuse reflectance spectra of the compounds **1**−**3** are investigated at room temperature and plotted in Figure 4. The spectra indicate a sharp absorption edge at about 2.10 eV for **1**, 2.18 eV for **2**, and 2.20 eV for **3**, respectively. As clearly depicted in Figure 4, the doping of alkali metal ions results in a blue shift of the absorption edges.

As stated above, the title compounds reveal a band gap in the visible light region, which is suitable for photocatalytic

DOI: 10.1021/acs.inorgchem.5b00652
Inorg. Chem. 2015, 54, 5874−5878

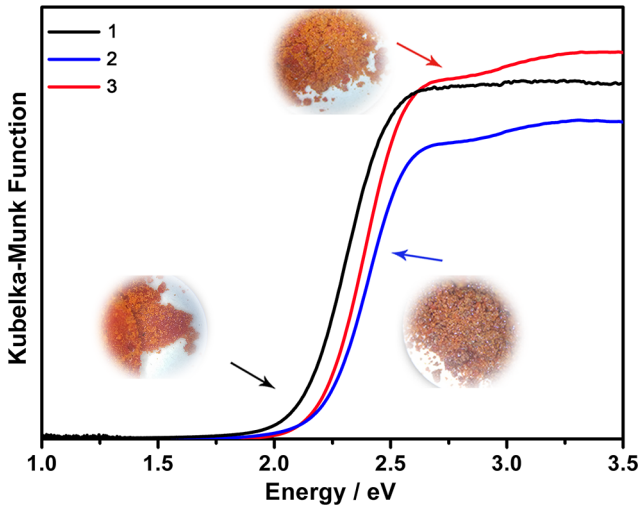

Figure 4. Solid-state optical absorption spectra of **1**–**3**.

applications. By choosing methyl orange (MO) and salicylic acid (SA) as test pollutants, the photodegradation performance of organic contaminants of the title compounds was evaluated under visible light irradiation. Temporal changes in the concentration of organic dyes were monitored by examining the variations of the intensities in the maximal absorption in UV–vis spectra (for details, see the Supporting Information). The maximal absorption was selected at about 464 and 508 nm in neutral, alkaline, and acidic conditions for MO and 296 nm for SA, respectively.

pH-dependent photocatalytic activity of **1** was carried out in MO solutions (0.25 g/L) at different pH values (pH = 1.5, 3, 4.5, 6.8, 8, 10, and 11.8). As shown in Figure 5, the degradation ratios of MO were 0.9% (pH = 6.8), 33.6% (pH = 4.5), 95.7% (pH = 3), and 79.5% (pH = 1.5), respectively, after 10 min under visible light illumination. Compared to that in neutral conditions (removal rate: 96% after 3 h), the photodegradation rate was accelerated (99% in 30 min for pH < 4.5) and was even 6 times faster when the pH was below 3 (Figure 5a; the results are also summarized in Table 2). While turning into a strong alkaline condition (pH = 11.8), the photodegradation was faster than those in neutral and weak alkaline conditions in the initial 30 min but terminated after 50 min. As a result of the pH variation, the title compound can retain stability over a wide pH range from 1.5 to 10 and the time for an entire MO decomposition is sharply reduced from 180 min at pH = 6.8 to 30 min at pH = 4.5, which is much faster than those of TiO_2 nanocrystals (removal rate: less than 10% after 5 h)[15] and comparable to those of noble metal-doped TiO_2 nanomaterials.[16] According to previous reports, the pH-dependent photodecomposition can mainly be attributed to the variations of surface charge properties of the photocatalyst.[17] The adsorption of MO is favored in the acidic solution due to its anionic configuration. As for the photodegradation process, the close contact of MO with the catalyst could facilitate its oxidative degradation by positive holes or hydroxyl radicals.[17a,b,18] In addition, MO becomes unstable in acidic conditions, which also makes the decolorization easier.[19] As shown in Figure 6, PXRD analysis after the selected experiments in the pH range from 1.5 to 10 demonstrates that there are no phase variations, indicating the high stability of compound **1** after the photocatalytic processes, whereas compound **1** decomposed into selenium and indium hydroxide after the photodegradation

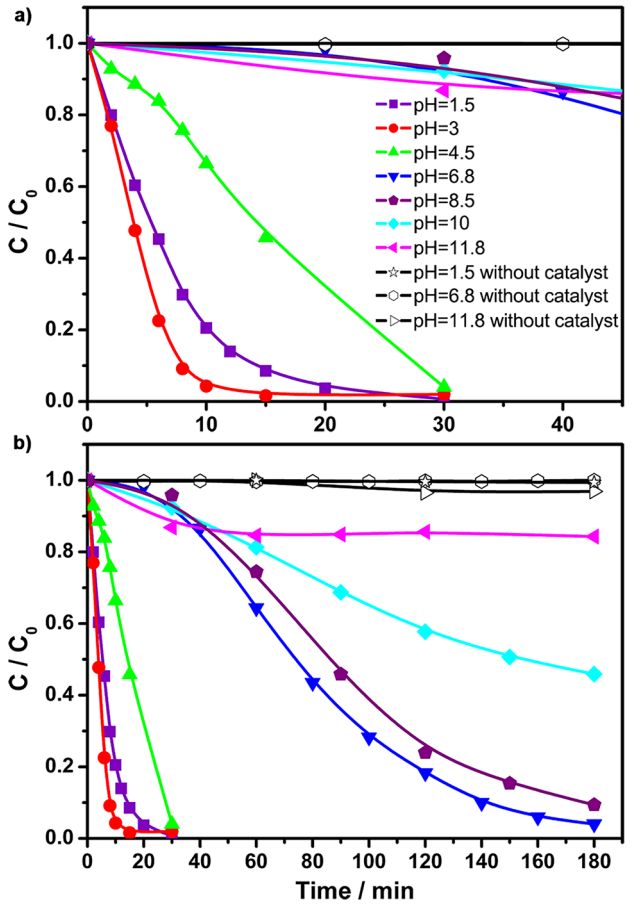

Figure 5. Photodegradation of MO in different pH values by compound **1** monitored as the normalized change in concentration as a function of irradiation time under visible light (Xe lamp, 420–780 nm). (a) The partial enlarged detail for the first 45 min of photodegradation process and (b) the full graph.

experiment at pH = 11.8, according to the PXRD pattern. For the doped compounds, the photodegradation rates of MO in neutral conditions are much slower compared to that of **1**, which were 58.8% and 70.7% after 3 h over **2** and **3**, respectively (Figure S10, Supporting Information). However, the stabilities of **2** and **3** after photodegradation experiments were also confirmed by PXRD (Figure S3, Supporting Information).

In addition, the photocatalytic activities of the catalysts have also been evaluated by decomposing the colorless substrates SA under visible light. However, no photodegradation of SA was observed, which implied that the photodegradation of organic dye may be through a self-sensitized mechanism.[20]

CONCLUSION

In conclusion, by means of a one-pot ionothermal method, we first obtained the ternary In-Sn-Se T2,2 cluster. Through a doping method, the alkali metal ions of Cs^+ and Rb^+ were successfully introduced into the central cavity of the as-prepared T2,2 cluster. The photodegradation performance of organic contaminants in different pH values shows that the title compounds have excellent stability and visible light photodegradation ability. The ordered distribution of dopant in a nanosized cluster provides an alternative way to prepare novel semiconductor materials with tunable properties.

DOI: 10.1021/acs.inorgchem.5b00652
Inorg. Chem. 2015, 54, 5874–5878

Table 2. pH-Dependent Photocatalytic Activities of 1 Toward MO Photodegradation[b]

	1.5	3	4.5	6.8	8.5	10	11.8
MO degradation (%) after 10 min illumination	79.5	95.7	33.6	*[a]	*[a]	*[a]	*[a]
MO degradation (%) after 30 min illumination	99.3	98.0	96.0	7.6	4.2	7.6	13.2
MO degradation (%) after 3 h illumination	*[a]	*[a]	*[a]	96.0	90.6	54.1	15.7

[a]"*" represents the data at the condition was not recorded. [b]Column headings are pH values.

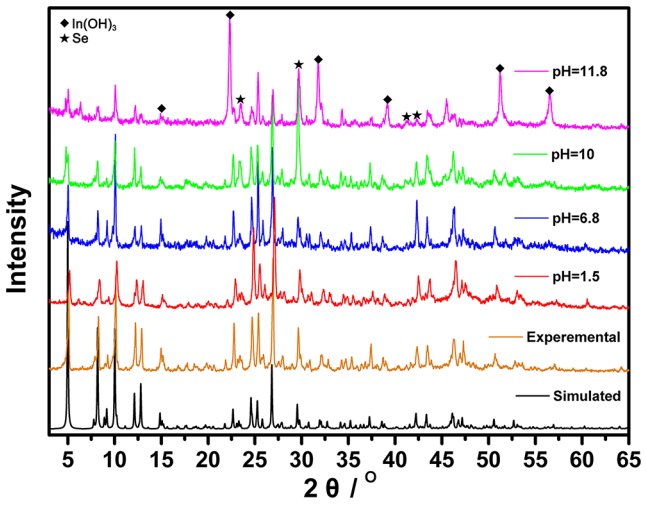

Figure 6. PXRD patterns for **1** before and after the selected photodegradation experiments in pH ranges from 1.5 to 11.8.

■ ASSOCIATED CONTENT

Supporting Information

Crystal structural data for **1**, **2**, and **3** in CIF format, additional structural details, PXRD, elemental analysis, TGA, EDX, ICP, and photocatalytic activity measurements. The Supporting Information is available free of charge on the ACS Publications website at DOI: 10.1021/acs.inorgchem.5b00652. Also available from the CCDC: 1049291 for **1**, 1049292 for **2**, and 1049293 for **3**.

■ AUTHOR INFORMATION

Corresponding Author

*E-mail: jrli@fjirsm.ac.cn. Fax: (+86)591−63173146.

Notes

The authors declare no competing financial interest.

■ ACKNOWLEDGMENTS

This work was supported by the 973 program (No. 2014CB845603) and the NNSF of China (Nos. 21371001 and 21221001).

■ REFERENCES

(1) (a) Alferov, Z. I. *Semiconductors* **1998**, *32*, 1−14. (b) Chung, D. Y.; Uher, C.; Kanatzidis, M. G. *Chem. Mater.* **2012**, *24*, 1854−1863. (c) Huang, X. Y.; Li, J.; Zhang, Y.; Mascarenhas, A. *J. Am. Chem. Soc.* **2003**, *125*, 7049−7055. (d) Dupuis, R. D.; Krames, M. R. *J. Lightwave Technol.* **2008**, *26*, 1154−1171.

(2) Fortunato, E.; Barquinha, P.; Martins, R. *Adv. Mater.* **2012**, *24*, 2945−2986.

(3) (a) Desnica, U. V. *Prog. Cryst. Growth Charact. Mater.* **1998**, *36*, 291−357. (b) Chen, X.; Shen, S.; Guo, L.; Mao, S. S. *Chem. Rev.* **2010**, *110*, 6503−6570. (c) Morkoc, H.; Strite, S.; Gao, G. B.; Lin, M. E.; Sverdlov, B.; Burns, M. *J. Appl. Phys.* **1994**, *76*, 1363−1398.

(4) Wu, T.; Zhang, Q.; Hou, Y.; Wang, L.; Mao, C.; Zheng, S. T.; Bu, X.; Feng, P. *J. Am. Chem. Soc.* **2013**, *135*, 10250−10253.

(5) Lin, J.; Zhang, Q.; Wang, L.; Liu, X.; Yan, W.; Wu, T.; Bu, X.; Feng, P. *J. Am. Chem. Soc.* **2014**, *136*, 4769−4779.

(6) (a) Riwotzki, K.; Haase, M. *J. Phys. Chem. B* **1998**, *102*, 10129−10135. (b) George, S.; Pokhrel, S.; Xia, T.; Gilbert, B.; Ji, Z. X.; Schowalter, M.; Rosenauer, A.; Damoiseaux, R.; Bradley, K. A.; Madler, L.; Nel, A. E. *ACS Nano* **2010**, *4*, 15−29. (c) Su, W. P.; Huang, X. Y.; Li, J.; Fu, H. X. *J. Am. Chem. Soc.* **2002**, *124*, 12944−12945.

(7) Soriano, R. B.; Arachchige, I. U.; Malliakas, C. D.; Wu, J. S.; Kanatzidis, M. G. *J. Am. Chem. Soc.* **2013**, *135*, 768−774.

(8) (a) Pfister, G. *J. Electron. Mater.* **1979**, *8*, 789−837. (b) Fan, F.-J.; Wu, L.; Yu, S.-H. *Energy Environ. Sci.* **2014**, *7*, 190−208. (c) Fu, H.; Tsang, S.-W. *Nanoscale* **2012**, *4*, 2187−2201. (d) Chen, G.; Seo, J.; Yang, C.; Prasad, P. N. *Chem. Soc. Rev.* **2013**, *42*, 8304−8338. (e) Lin, J.; Dong, Y.; Zhang, Q.; Hu, D.; Li, N.; Wang, L.; Liu, Y.; Wu, T. *Angew. Chem., Int. Ed.* **2015**, *54*, 5103−5107.

(9) (a) Reichert, W. M.; Holbrey, J. D.; Vigour, K. B.; Morgan, T. D.; Broker, G. A.; Rogers, R. D. *Chem. Commun.* **2006**, 4767−4779. (b) Wilkes, J. S. *Green Chem.* **2002**, *4*, 73−80. (c) Huddleston, J. G.; Visser, A. E.; Reichert, W. M.; Willauer, H. D.; Broker, G. A.; Rogers, R. D. *Green Chem.* **2001**, *3*, 156−164.

(10) Xiong, W. W.; Li, J. R.; Hu, B.; Tan, B.; Li, R. F.; Huang, X. Y. *Chem. Sci.* **2012**, *3*, 1200−1204.

(11) (a) Wendlandt, W. M.; Hecht, H. G. *Reflectance Spectroscopy*; Interscience: New York, 1966. (b) Zhang, J.; Xi, J.; Ji, Z. *J. Mater. Chem.* **2012**, *22*, 17700−17708.

(12) Sheldrick, G. M. *Acta Crystallogr., Sect. A* **2008**, *64*, 112−122.

(13) Li, H. L.; Kim, J.; O'Keeffe, M.; Yaghi, O. M. *Angew. Chem., Int. Ed.* **2003**, *42*, 1819−1821.

(14) (a) Zheng, N.; Bu, X.; Wang, B.; Feng, P. *Science* **2002**, *298*, 2366−2369. (b) Zheng, N. F.; Bu, X. H.; Feng, P. Y. *Nature* **2003**, *426*, 428−432.

(15) Ruan, S. P.; Wu, F. Q.; Zhang, T.; Gao, W.; Xu, B. K.; Zhao, M. Y. *Mater. Chem. Phys.* **2001**, *69*, 7−9.

(16) (a) Tian, B.; Dong, R.; Zhang, J.; Bao, S.; Yang, F.; Zhang, J. *Appl. Catal., B* **2014**, *158−159*, 76−84. (b) Arabatzis, I. M.; Stergiopoulos, T.; Bernard, M. C.; Labou, D.; Neophytides, S. G.; Falaras, P. *Appl. Catal., B* **2003**, *42*, 187−201.

(17) (a) Kisch, H. *Angew. Chem., Int. Ed.* **2013**, *52*, 812−847. (b) Colmenares, J. C.; Luque, R. *Chem. Soc. Rev.* **2014**, *43*, 765−778. (c) Bae, S.; Kim, S.; Lee, S.; Choi, W. *Catal. Today* **2014**, *224*, 21−28.

(18) Hoffmann, M. R.; Martin, S. T.; Choi, W.; Bahnemann, D. W. *Chem. Rev.* **1995**, *95*, 69−96.

(19) Lin, X.; Huang, F.; Wang, W.; Wang, Y.; Xia, Y.; Shi, J. *Appl. Catal., A* **2006**, *313*, 218−223.

(20) (a) Cho, Y. M.; Choi, W. Y.; Lee, C. H.; Hyeon, T.; Lee, H. I. *Environ. Sci. Technol.* **2001**, *35*, 966−970. (b) Alexander, M. V.; Rosentreter, J. J. *Microchem. J.* **2008**, *88*, 38−44. (c) Bae, E.; Choi, W. *Environ. Sci. Technol.* **2003**, *37*, 147−152.

DOI: 10.1021/acs.inorgchem.5b00652
Inorg. Chem. 2015, 54, 5874−5878